Contribution to the book "Remote Sensing of the Cryosphere" Chapter: Gravimetry Measurements From Space

Scott B. Luthcke,[1*] D.D. Rowlands,[1] T.J. Sabaka,[1]
B.D. Loomis,[2] M. Horwath,[3] A.A. Arendt,[4]

[1] *NASA Goddard Space Flight Center, Planetary Geodynamics Laboratory, Greenbelt, MD*
[*] *E-mail: scott.b.luthcke@nasa.gov*
[2] *SGT Inc., Science Division, Greenbelt, MD*
[3] *Technische Universitat Munchen, Munich, Germany*
[4] *University of Alaska, Fairbanks, AK*

ABSTRACT.

INTRODUCTION

Since its launch in March of 2002, the Gravity Recovery and Climate Experiment (GRACE) mission has acquired ultra-precise inter-satellite K-band range and range-rate (KBRR) measurements taken between two co-orbiting satellites in a 450 km altitude polar orbit, approximately 220 km apart (Tapley and others, 2004). These data have vastly improved our knowledge of the Earth's time-variable gravity field. In particular the GRACE mission has been instrumental in quantifying present day terrestrial ice mass evolution (*e.g.* Luthcke and others, 2006a, 2008; Velicogna, 2009; Chen and others, 2011; Schrama and Wouters, 2011; Jacob and others, 2012; King and others, 2012). The purpose of this chapter is to provide the reader with an understanding of the GRACE mission, its fundamental measurements and how those measurements are used to observe the Earth's surface mass flux, and in particular, terrestrial ice mass evolution.

OBSERVING THE EARTH'S GRAVITY FIELD WITH INTER-SATELLITE RANGING

From the beginning of the space age, observations of satellite motions have been used to compute gravity models of the Earth. Over the decades there have been several important geopotential model development efforts based on satellite tracking data from a suite of Earth orbiting satellites, for example Lemoine and others (1998). The motion of a satellite is computed by modeling the conservative and non-conservative forces acting on the satellite and integrating the resultant differential equations to obtain a time series of predicted position and velocity (ephemeris). The force models (including the Earth's gravitational potential field) are then refined through parameter estimation minimizing a measure of the difference between the computed tracking data observations, constructed from the estimated time series of satellite position and velocity, and the observed tracking data. Some examples of modern satellite tracking data for Precision Orbit Determination (POD) and geodetic parameter estimation include: Satellite Laser Ranging (SLR), Global Positioning System (GPS) satellite-satellite ranging through carrier and code phase observations, and Doppler Orbitography and Radiopositioning Integrated by Satellite (DORIS) (Luthcke and others, 2003).

Milo Wolff was the first to introduce the concept of computing the variations in the Earth's gravity field directly from observations of the changing range between two low earth co-orbiting satellites (M Wolff, 1969). The motion of a satellite is dependent on the gravitational potential, which can be understood using conservation of energy. Ignoring non-conservative forces (e.g. drag and radiation pressure), changes in the Earth's potential energy must be compensated by a change in energy from another component. These components include a change in kinetic energy in the three orthogonal velocity directions (e.g. radial, line-of-sight between satellites, and orthogonal to the first two), and a potential energy change due to change in radial position of the satellites. M Wolff (1969) showed that the change in kinetic energy in the line-of-sight direction between the two co-orbiting satellites is by far the dominant mode of energy compensation. Given the simplifying assumptions of the two satellites in a perfectly circular co-orbit, and ignoring non-conservative forces, the line-of-sight range-rate between the satellites can be expressed as:

$$\dot{\rho}_{12} = \frac{1}{V} U_{12} \tag{1}$$

where V is the mean orbital velocity given by $(\frac{GM}{R})^{\frac{1}{2}}$, and U_{12} is the potential difference between satellite position 1 and satellite position 2.

The differential potential can be expressed as:

$$U_{12} = U_{12}^{Earth} + U_{12}^{N-body} + U_{12}^{tides} + U_{12}^{oceans} + U_{12}^{atmosphere} + U_{12}^{hydrology} + U_{12}^{land\ ice} + \epsilon \quad (2)$$

Spatial and temporal contributions to the potential include: solid Earth, planetary bodies, ocean tides, solid Earth and pole tides, and mass changes due to the oceans, atmosphere and land ice. Of course simplifying assumptions can not be used in precisely computing the Earth's time variable gravity field. Therefore, in order to isolate the land ice surface mass changes, it is necessary to compute and model: the position and velocity of the satellites, their orientation to get the line-of-sight pointing, the non-conservative forces, and all of the potential contributions noted above including glacial isostatic adjustment, tides, and ocean and atmosphere mass redistribution.

The GRACE project provides Level 1B (L1B) data which includes: (1) the GPS tracking range and phase observations as well as the position and velocity of the satellites, and timing of observations determined from the GPS tracking, (2) the orientation of the satellites with respect to the inertial frame as a time series of quaternions determined from the onboard star cameras, (3) observations of all non-conservative forces from the onboard accelerometers, and (4) inter-satellite biased range, range-rate and range-acceleration observations (along with important light time and geometric corrections) from the onboard K-band ranging system. For an excellent detailed discussion of the GRACE L1B data product the reader is directed to the "GRACE Level 1B Data Product User Handbook" (Case and others, 2010).

Time variable gravity is obtained as a time series of delta corrections to an *a priori* geopotential model. The typical time step is on the order of monthly to 10 days. The geopotential delta corrections are estimated by minimizing a measure of the difference between computed inter-satellite ranging observations, based on the *a priori* geopotential, and the observed inter-satellite ranging data provided by the GRACE L1B product. As discussed in detail in the next section, the geopotential corrections can be formulated as either a time series of delta Stokes coefficients or surface mass concentration parameters expressed in equivalent centimeters of water height for a specified area. The L1B data are processed in a "state of the art" precision orbit determination and geodetic parameter estimation system such as NASA Goddard Space Flight Center's GEODYN. These systems provide the necessary reference frame, satellite dynamics, and force modeling infrastructure to compute the inter-satellite ranging residuals (difference between the computed and observed) and the partial derivatives of the delta geopotential parameters with respect to the inter-satellite ranging. The GRACE mission L1B data processing centers [Jet Propulsion Laboratory (JPL), CA; Center for Space Research (CSR), TX; GeoForschungszentrum (GFZ), Potsdam, Germany] all use their own sophisticated processing systems, but for the purposes of this chapter, we will use the GEODYN system and processing approach.

The contributions to the computed inter-satellite ranging observations from the Earth's static gravity field, planetary bodies, ocean tides, solid Earth and pole tides are computed within GEODYN. GEODYN is also used to calibrate the accelerometer data in order to compute the contribution of non-conservative forces (Luthcke and others, 2006b). The contributions from atmospheric and ocean mass variations, and in particular high frequency variations that would otherwise alias the longer-term (10-30 days) estimated geopotential corrections, must be accounted for during the computation of the inter-satellite ranging residuals and partial derivatives. This is accomplished during the L1B data processing through forward modeling, either using the GRACE mission Atmosphere and Ocean De-aliasing Level 1B data product (AOD1B) (Flechtner, 2007), or a comparable atmosphere and ocean forward model (Luthcke and others, 2006b).

SURFACE MASS VARIABILITY FROM GRACE

The time variable gravitational potential of the Earth can be expressed as a delta geopotential from the static geopotential and any time varying gravitational effects one wishes to forward model as noted in Eq. 2, and discussed above. For any point on, or above, the surface of the Earth, the time dependent delta gravitational potential can be expressed in a spherical harmonic expansion, assuming the total mass of the Earth system is time invariant (Hoffmann-Wellenhof and Moritz, 2005):

$$\Delta U(r,\lambda,\phi,t) = \frac{GM}{R}\sum_{l=0}^{l_{max}}\sum_{m=0}^{l}\left(\frac{R}{r}\right)^{l+1}\bar{P}_{lm}(\sin\lambda)\{\Delta\bar{C}_{lm}(t)\cos(m\phi) + \Delta\bar{S}_{lm}(t)\sin(m\phi)\}. \quad (3)$$

where

ΔU	Delta gravitational potential.
$r, \lambda,\ \phi$	Spherical geocentric coordinates of computation point (radius, latitude, longitude).
GM	The product of the gravitational constant and the mass of the Earth.
R	Mean semi-major axis of the Earth.
l, m	Degree and order of spherical harmonic.
$\bar{P}_{lm}$	Normalized associated Legendre polynomials.
$\Delta\bar{C}_{lm}(t), \Delta\bar{S}_{lm}(t)$	Delta Stokes' coefficients fully normalized.

The GRACE data centers process the L1B data, and estimate delta gravitational potential fields (gravity fields) from the reduction of the inter-satellite ranging residuals as discussed in the previous section. This Level-2 data product is provided to the public most typically as a time series of spherical harmonic (SH) (Stokes) coefficients. For example, the University of Texas Center for Space Research (CSR) Release-5 Level 2 product is a time series of monthly SH coefficients up to degree and order 60 (Bettadpur and others, 2012). These fields have the atmosphere and oceans mass variations removed as the AOD1B atmosphere and ocean model product was forward modeled in the processing of the L1B data. The gravity fields are estimated in the Earth's center of mass frame, and therefore, the degree 1 SH coefficients are zero.

Temporal variations of the gravity field are primarily driven by the global redistribution of water mass that occurs at or near the surface of the Earth. These changes in surface mass are often expressed as changes in density of a thin layer at the Earth's surface. Eq. 4 relates the delta Stokes coefficients of Eq. 3 to the change in surface density, $\Delta\sigma$, at a point on the Earth's surface.

$$\Delta\sigma(\lambda,\phi,t) = \frac{M}{4\pi R^2}\sum_{l=0}^{l_{max}}\sum_{m=0}^{l}\bar{P}_{lm}(\sin\lambda)\frac{2l+1}{1+k'_l}\{\Delta\bar{C}_{lm}(t)\cos(m\phi)+\Delta\bar{S}_{lm}(t)\sin(m\phi)\}. \tag{4}$$

where

k'_l Loading Love number of degree l, to account for the Earth's elastic yielding which in general counteracts the additional surface density.

The surface density change, $\Delta\sigma$, has units of kg/m^2, and can be converted to centimeters of equivalent water height by noting that the density of water is 1000 kg/m^3: $\Delta H(t) = \Delta\sigma/10$.

Although Eq. 4 is rigorously correct, it can not be used with delta Stokes coefficients estimated from GRACE to compute surface mass density at individual point locations. Two problems with the GRACE SH coefficients prevent this. The first problem is significant north-south striping artifacts as illustrated in Figure 1 . The meridional striping patterns observed in Figure 1 are due to the aliasing effects of unmodeled short-term temporal variations (Swenson and Wahr, 2006; Klees and others, 2008). Over a given GRACE solution period (e.g. one month), the SH coefficient increments that are adjusted with respect to the background model are assumed to be constant, and therefore mass changes within the solution period that are not modeled cannot be captured by this adjustment. In part, they are absorbed by the adjusted spatial variations, thus introducing artifacts into the solution that typically appear as stripes following the orbital sampling pattern. The magnitude of the stripes are reduced as you approach the poles due to the fact that the orbit tracks converge at the pole, and therefore the spatio-temporal sampling is significantly better minimizing aliasing. Improvements in the atmospheric and oceanic models and strategies to account for short-term variations in the gravity adjustment are approaches being pursued to mitigate the effects of aliasing.

The second problem associated with the direct use of Eq. 4 is signal leakage, which has multiple causes. The primary cause is the finite expansion used in Eq. 4 (usually lmax=60 for time variable gravity derived from GRACE). Consider the delta stoles coefficients that represent a change in mass corresponding to an extra 1 cm of water standing over a 1x1 arc-degree region. If this set of coefficients is truncated at degree 60, the total mass is correct but it is spread out past the original region boundaries. Signal has leaked out, leaving less in the original area.

For these reasons, GRACE data are most commonly used to quantify the mass changes within a particular region, such as an ice sheet or drainage basin. Using Eq. 4 to get an average value over a substantial area diminishes striping and leakage. The process of averaging is further improved with filtering techniques to mitigate striping and leakage. The average surface density change over a region can be obtained by the following expression (Swenson and Wahr, 2002):

$$\overline{\Delta\sigma_{region}}(\lambda,\phi,t) = \frac{1}{\Omega_{region}}\int\Delta\sigma(\lambda,\phi,t)\vartheta(\lambda,\phi)d\Omega, \tag{5}$$

where $\vartheta(\lambda,\phi)$ is defined as 1 inside the region and 0 outside, $d\Omega = \cos\lambda\, d\lambda\, d\phi$ is an element of solid angle, and Ω_{region} is the angular area of the region. Combining Eqs. 4 and 5, this can be rewritten as (Swenson and Wahr, 2002):

$$\overline{\Delta\sigma_{region}}(\lambda,\phi,t) = \frac{M}{4\pi R^2\Omega_{region}}\sum_{l=0}^{l_{max}}\sum_{m=0}^{l}\frac{2l+1}{1+k'_l}\{\vartheta^C_{lm}\Delta\bar{C}_{lm}(t)+\vartheta^S_{lm}\Delta\bar{S}_{lm}(t)\}, \tag{6}$$

where ϑ^C_{lm} and ϑ^S_{lm} are the spherical harmonic coefficients that describe $\vartheta(\lambda,\phi)$ which are related by:

$$\vartheta(\lambda,\phi) = \frac{1}{4\pi}\sum_{l=0}^{l_{max}}\sum_{m=0}^{l}\bar{P}_{lm}(\sin\lambda)\{\vartheta^C_{lm}\cos(m\phi)+\vartheta^S_{lm}\sin(m\phi)\}, \tag{7}$$

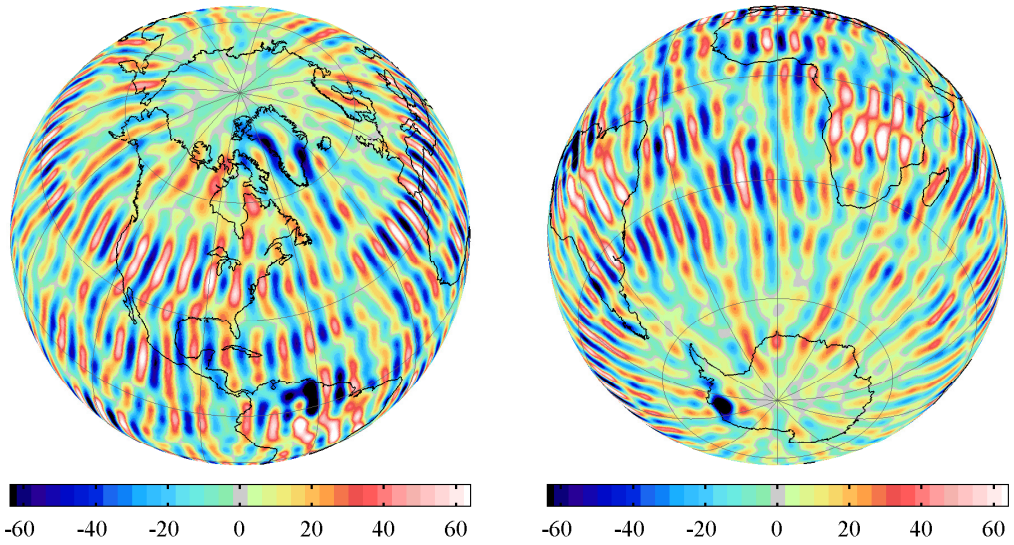

Fig. 1. Surface mass anomaly from the mean for March 2010 computed directly from CSR RL05 Level-2 monthly spherical harmonics.

$$\left\{ \begin{array}{c} \vartheta^C_{lm} \\ \vartheta^S_{lm} \end{array} \right\} = \int \vartheta(\lambda,\phi) \bar{P}_{lm}(\sin\lambda) \left\{ \begin{array}{c} \cos(m\phi) \\ \sin(m\phi) \end{array} \right\} d\Omega. \tag{8}$$

As l_{max} approaches infinity, Eqs. 5 and 6 yield nearly identical results. For the $l_{max} = 60$ case, Eq. 6 may reduce signal attenuation and leakage for a particular area of interest. In Eq. 4, $\Delta\sigma$ truncated to degree 60 has leakage problems and is integrated only over the area of interest. The $\vartheta(\lambda,\phi)$ function computed in Eq. 7 also has leakage problems and extends out past the original area of interest. Furthermore, Eq. 7 gives a form that is convenient for filtering with averaging kernels.

The most common method for extracting localized mass variations from the GRACE project SH coefficients is to apply an averaging kernel, $\overline{W}(\lambda,\phi)$, in Eq. 6 in place of $\vartheta(\lambda,\phi)$ (Swenson and Wahr, 2002). This kernel is computed by convolving the exact kernel, $\vartheta(\lambda,\phi)$, with a Gaussian filter, resulting in a kernel that smoothly changes from a value of 1 inside the region, to a value of 0 outside the region, over a distance approximately equal to the design smoothing radius. As with the filtering of the global SH coefficients mentioned above, the motivation here is to extract as much signal as possible while reducing the effect of the errors at the highest degrees. It is important that this averaging kernel be calibrated to account for the fact that the smoothing function attenuates the signal. The computed calibration factor typically has a value slightly greater than one. It should be noted that the application of the averaging kernel introduces a leakage of signal from outside the region of interest which is caused by the fact that $\overline{W}(\lambda,\phi)$ is an approximation of $\vartheta(\lambda,\phi)$.

Typically the noise covariance of the estimated Stokes coefficients are not taken into account in the post-solution filtering methods, and therefore they are not optimal filters (Klees and others, 2008). Signal attenuation, limited spatio-temporal resolution, and signal leakage in and out of the domain of interest are particular problems when applying the filtering methods. An alternative method is to estimate surface mass concentrations (mascons) directly from the reduction of the GRACE inter-satellite range-rate observation residuals. The mascon technique uses geolocatable anisotropic constraints to estimate the global mass change directly from GRACE KBRR data, accounting for the full Stokes noise covariance (Luthcke and others, 2006a, 2008; Rowlands and others, 2010; Sabaka and others, 2010; Luthcke and others, 2013). Mascon parameters can be derived using the following relationship that a change in the gravitational potential caused by adding a small uniform layer of mass over a region at an epoch t can be represented as a set of (differential) potential coefficients which can be added to the mean field. The delta coefficients can be computed as in Chao and Au (1987):

$$\Delta\bar{C}_{lm}(t) = \left\{ \frac{10(1+k'_l)R^2}{(2l+1)M} \int \bar{P}_{lm}(\sin\lambda)\cos m\phi \; d\Omega \right\} \Delta H(t), \tag{9}$$

$$\Delta\bar{S}_{lm}(t) = \left\{ \frac{10(1+k'_l)R^2}{(2l+1)M} \int \bar{P}_{lm}(\sin\lambda) \sin m\phi \; d\Omega \right\} \Delta H(t) \tag{10}$$

Following Rowlands and others (2005), the estimated mascon parameter, $H_j(t)$, for each mascon area j is a scale factor on the set of differential Stokes coefficients for that mascon area, giving a surface mass change in equivalent centimeters of water. Assembling in matrix notation over j mascons using the above equations, provides a set of partial derivatives, L, of the differential Stokes coefficients, $\Delta\mathbf{s}$, with respect to equivalent water height, $\Delta\mathbf{h}$, such that

$$\Delta\mathbf{s} = \mathrm{L}\,\Delta\mathbf{h}. \tag{11}$$

The matrix L is precomputed one time for the defined set of mascons using Eqs. 9 and 10 and setting $\Delta H(t)$ to unity.

Standard processing of GRACE L1B KBRR data is usually geared to the estimation of differential Stokes coefficients that represent global change over a chosen time period, such as the GRACE project monthly spherical harmonic products. In orbital softwares like GEODYN that estimate Stokes coefficients from KBRR data, the partial derivative of each KBRR observation with respect to every estimated Stokes coefficient are routinely computed. To change the parameterization from global Stokes coefficients to local mascons, all that is required is to compute the partial derivative of each KBRR observation with respect to all of the local mascons. This is accomplished with a change of basis using the matrix L defined above to post-multiply the matrix of partial derivatives of the KBRR observations with respect to the Stokes coefficients normally computed in the L1B data processing (see Eq. 12).

With the change of basis, L, it is then easy to convert the process of estimation of Stokes coefficients to the estimation of mascons. Some researchers, for example Jacob and others (2012), use L to estimate mascons from GRACE level 2 Stokes coefficients instead of from the original KBRR observations. This is an alternative to the averaging kernel approach described earlier (Eqs. 6 - 8). The mass distribution described by the matrix L is not a step function of 1 cm water over the area of a mascon set of interest, because it is typically truncated to degree 60 limited by the fundamental resolution of the GRACE observations. This is an advantage when recovering signal leakage out, because L effectively pulls back the signal into the intended mascon region during the estimation process. However, there is now the issue of leakage of signal in from surrounding regions. As described further below, these leakage problems are further mitigated applying spatial constraints in the mascon estimation process.

The mascon parameters are non-linear functions of the GRACE inter-satellite K-band range-rate (KBRR) observations, and are therefore estimated using a non-linear least squares Gauss-Newton (GN) method (Seber and Wild, 1989). The application of the GN method to the estimation of the mascon parameters at iteration k, can be expressed following Sabaka and others (2010); Luthcke and others (2013):

$$\text{GN iteration } k \left\{ \; \tilde{\mathbf{h}}_{k+1} = \left(\mathrm{L}^{\mathrm{T}}\mathrm{A}^{\mathrm{T}}\mathrm{WAL} + \mu \mathrm{P}_{hh} \right)^{-1} \mathrm{L}^{\mathrm{T}}\mathrm{A}^{\mathrm{T}}\mathrm{W} \left(\mathbf{r} + \mathrm{AL}\tilde{\mathbf{h}}_k \right) \right. \tag{12}$$

where

$\tilde{\mathbf{h}}_{k+1}$	Update of mascon parameters in equivalent cm of water.
L	Partial derivatives of the differential Stokes coefficients with respect to the mascon parameters.
A	Partial derivatives of KBRR observations with respect to the Stokes coefficients .
W	Data weight matrix which accounts for measurement noise and orbital arc parameters.
P_{hh}	mascon regularization matrix.
μ	Regularization matrix damping parameter.
r	KBRR residuals; difference between observations and model prediction.

The above is an optimal filter taking into account the noise covariance. A regularization matrix is used, which is constructed from anisotropic constraints that are applied using geophysical boundaries. The constraints are constructed in groups that represent geographical regions, so that if two mascons reside within the same region, the constraint weight is a simple exponential function of the distance and time between the two mascons. If two mascons reside in different regions the weight is zero and the constraint vanishes. The result is a smoothed solution that limits leakage across regional boundaries (e.g. Greenland ice sheet or Gulf of Alaska glacier region). Furthermore, the solution is iterated while minimizing the KBRR observation residuals to recover the full signal and minimizing attenuation (Luthcke and others, 2013). Figure 2 shows the monthly surface mass anomaly from a recent iterated global mascon solution (Luthcke and others, 2013). The improvements in signal to noise, due to the regularization and iteration applied in the estimation of the global mascons from the minimization of the GRACE KBRR data, can be seen in comparing with Figure 1.

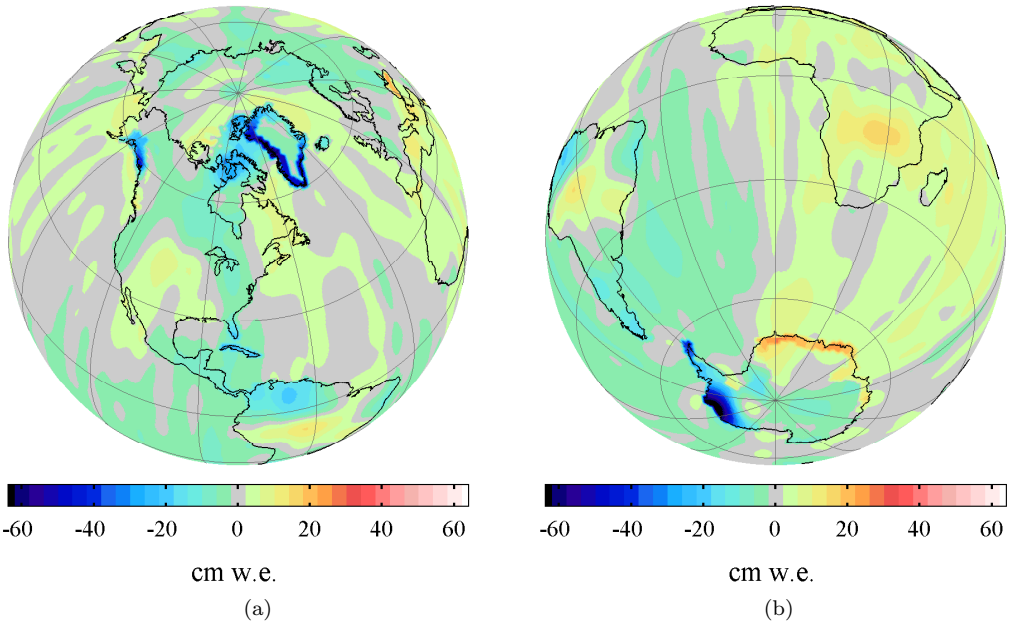

Fig. 2. Surface mass anomaly from the mean for March 2010 computed from a recent global mascon solution (Luthcke and others, 2013).

In addition to the mitigation of signal attenuation and leakage, there are additional challenges in extracting ice sheet and glacier region mass balance from GRACE. The GRACE observations measure all contributions to the Earth's temporal and spatial mass variability. Therefore, it is necessary to remove the non-glacier signals through independent datasets and models. Models of tidal effects, as well as non-tidal atmospheric and oceanic mass redistributions are already employed in the gravity field processing in order to minimize aliasing of the high frequency mass change signals, thus removing these signals from the gravity field solutions within their model errors (Flechtner, 2007; Bettadpur and others, 2012). In many terrestrial ice applications Glacial Isostatic Adjustment (GIA) and terrestrial water storage (TWS) signals are significant in comparison to the ice signals themselves, and therefore must be removed and accounted for in the error analysis (Shepherd and others, 2012; Luthcke and others, 2008). Errors in the atmosphere and ocean forward modeling must also be considered.

RESULTS

A comprehensive review of the many applications of GRACE data to cryospheric science, over the course of nearly a decade, is beyond the scope of this chapter. However, to illustrate the power of the GRACE observations to observe terrestrial ice mass evolution we summarize the results from a global mascon solution (Luthcke and others, 2013) that was used in the international Ice Mass Balance Intercomparison Exercise (IMBIE) (Shepherd and others, 2012). It is important to note that for the duration of the GRACE mission, the processing procedures have been continually enhanced, and more accurate forward models have become available, resulting in improved time variable gravity solutions and science products. As the processing methods and models continue to improve, and the time series of data continues to grow, it is acknowledged that the results now presented will also be updated and improved.

Here we summarize the mascon solution presented in Luthcke and others (2013). The mascons are estimated globally with 10-day temporal and 1-arc-degree equal area spatial sampling. The ice sheet mascons are restricted to grounded ice zones, and grouped according to major ice regions, applying anisotropic constraints as discussed in the previous section. Mass variations from tides, oceans, atmosphere, and hydrology are forward modeled. For both the Greenland Ice Sheet (GIS) and Gulf of Alaska glaciers (GOA), a GIA model based on the ICE-5G deglaciation history and an incompressible 2-layer approximation to the VM2 viscosity profile is used to correct the GRACE mascon solution (Paulson and others, 2007, computed and provided by Geruo A). For the Antarctic Ice Sheet (AIS), the IJ05_R2 regional GIA model is used (Ivins and others, 2012). The mascon solutions are corrected for the viscous component of post- Little Ice Age (LIA) GIA following the collapse of the Glacier Bay Icefield. As in Luthcke and others (2008), a regional post-LIA GIA model is applied that is rigidly constrained by approximately 100 precise GPS and Relative Sea Level (RSL) observations of uplift (Larsen and others, 2005). The mascon solutions are further corrected to reflect surface mass variability in the Earth's center of figure frame rather than the center of mass frame in which the solutions are performed. The geocenter correction used in the IMBIE study (Shepherd and others, 2012), derived from the degree 1 Stokes coefficients determined from Swenson and others (2008), is applied. The geocenter correction accounts

for approximately 1% of the GIS and GOA ice trends, and less than 3% for the West AIS and AIS Peninsula ice trends. The largest impact of the geocenter correction is for East AIS at 17% of the trend.

The mascon solution results are summarized in Figures 3 and 4 for the five most important terrestrial ice regions in terms of contribution to sea level rise: GIS, GOA, East, West and Peninsula regions of the Antarctic Ice Sheet (EAIS, WAIS, and AISP). The figures show mass change results for Apr. 1, 2003 – Dec. 1, 2010, while all reported mass trends are computed over the span of integer number of years: Dec. 1, 2003 – Dec. 1, 2010. It is also important to note that mean annual balances do not exactly match the mass trends, as they are computed over slightly different time periods (Luthcke and others, 2013). A detailed discussion of these results is provided in Luthcke and others (2013), while here we simply point to a few highlights.

The most important contribution of GRACE to cryospheric sciences is the excellent temporal resolution of mass change observable over the entire areas of the ice sheets and glacier regions. Observations of changes in mass ranging from $\sim$ 15 days to seasonal, annual and decadal are possible using GRACE. GRACE has quantified not only the long-term trends of terrestrial ice, but also the seasonal and inter-annual balance. Referencing Figures 3 and 4, we see the GIS is dominated by long-term negative mass trend from the low elevation margins of the ice sheet. The losses are largest from both the Jakobshavn glacier region on the west coast and the Helheim glacier region on the east coast. The observed mass trend of the GIS over this time period is -230 $\pm$ 12 Gt a^{-1}. The error bars include the contributions from the mascon solution itself, forward modeling and correction errors, and signal leakage in and out of the region of interest (Luthcke and others, 2013). Significant annual balance anomalies are observed for the 2004 balance year (positive) and the 2010 balance year (negative), giving rise to an apparent -10 $\pm$ 6 Gt a^{-2} acceleration of mass loss.

Unlike the GIS, both the magnitude and uncertainties of the GIA corrections for the AIS are significant with respect to the total trend. The overall AIS trend for the 2003.12 to 2010.12 time period studied is -81 $\pm$ 26 Gt a^{-1}. The AIS trend is dominated by significant mass loss from the WAIS with a trend of -106 $\pm$ 16 Gt a^{-1}. A trend of -38 $\pm$14 Gt a^{-1} is found for the AIS Peninsula, while EAIS trend is 63 $\pm$ 28 Gt a^{-1}. The largest long term mass losses are found in the WAIS along the Amundsen and Bellingshausen Sea coasts, concentrated along the Pine Island embayment, and at the northern tip of the Peninsula. The WAIS is of particular concern for sea level rise, as this region exhibits the largest accelerated mass loss at -46 $\pm$ 6 Gt a^{-2}. While inter-annual variability of the WAIS annual balances is observed, there is a consistent negative trend in these data (see Figs. 3 and 4), which represents the largest persistent multi-year acceleration of mass loss. The EAIS shows a significant 2009 positive annual balance concentrated along the Queen Maud Land and Wilkes land coasts due to a significant accumulation anomaly (Luthcke and others, 2013; Shepherd and others, 2012). The EAIS, WAIS and AISP all show very significant annual balance anomalies relative to the mean annual balance with anomalies in some years notably larger than the mean annual balance. This is in contrast to the GIS where annual balance anomalies are only a fraction of the mean annual balance.

Even with twenty times less ice covered area than the GIS, the GOA glaciers have lost mass at a significant rate of -69 $\pm$ 11 Gt a^{-1} for the time period 2003.12 to 2010.12, and a mean annual balance of -77 $\pm$ 11 Gt a^{-1} for the balance years 2004-2010. The largest mass losses occur in the St. Elias and Glacier Bay regions, and the GOA region as a whole exhibits significant inter-annual and seasonal variation compared to the long-term trend (Figure 4). What is of particular interest is the rapid response of the GOA region to climate change. Large negative annual mass balance anomalies are observed in 2004 due to record warm temperatures across the region (Truffer and others, 2005), and 2009 most likely attributed to the March 31, 2009 eruption of Mt. Redoubt. The eruption spread volcanic ash across much of the GOA region (Schaefer and others, 2012) likely enhancing melt rates through a reduction in surface albedo (Arendt and others, submitted). The large positive annual balance anomaly observed in 2008 is the result of the large 2007-08 winter accumulation followed by a cool 2008 summer season.

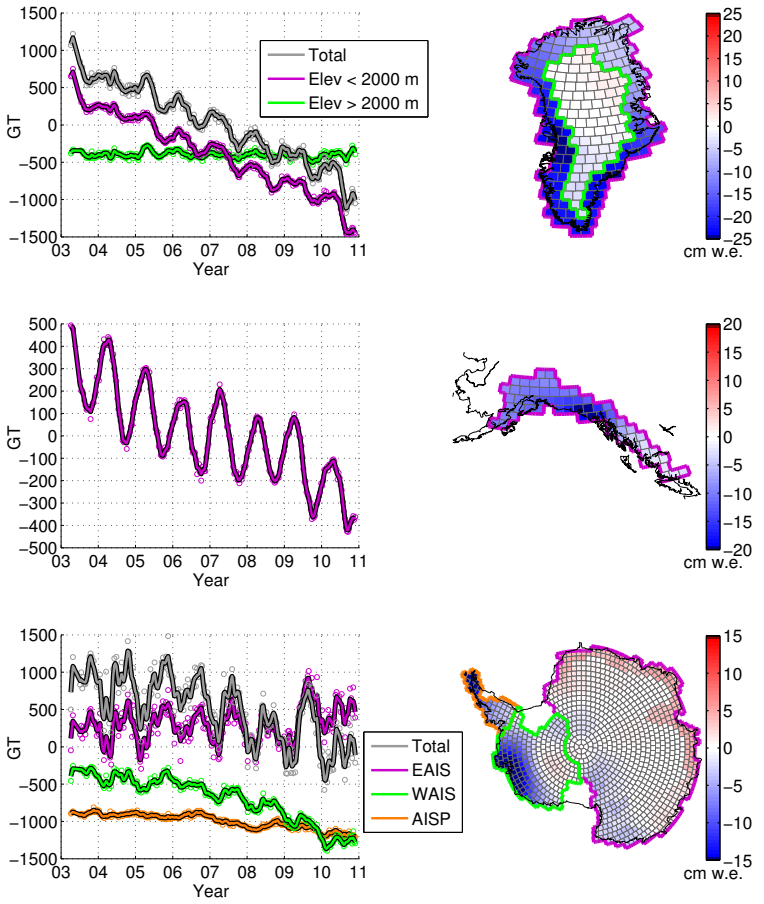

Fig. 3. Regional land ice mass change and spatial maps of annual mass balance.

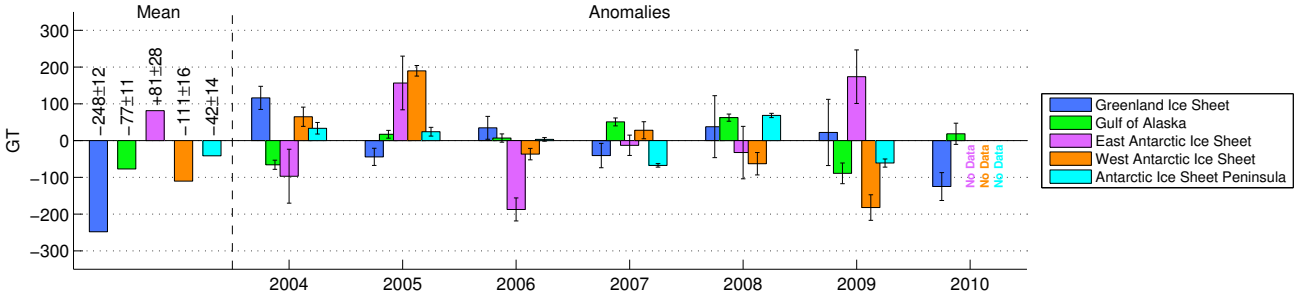

Fig. 4. Mean and anomalies of annual (net) mass balances by region.

REFERENCES

Arendt A, Luthcke S, O'Neel S, Gardner A, Hill D and Abdalati W, submitted. Validation of a GRACE global mascon Solution for Gulf of Alaska Glaciers.

Bettadpur S and the CSR Level-2 Team (2012) Assessment of GRACE mission performance and the RL05 gravity fields. *Paper G31C-02, AGU Fall Meeting, San Francisco, CA*

Case K, Kruisinga G, and Wu SC (2010) GRACE Level 1B Data Product User Handbook. *JPL D-22027, Jet Propulsion Laboratory, CA, USA*

Chao BF and Au A (1987) Snow Load Effect on the Earth's Rotation and Gravitational Field, 1979–1985. *J. Geophys. Res.*, **92**(B9), 9415–9422

Chen JL, Wilson CR, and Tapley BD (2011) Interannual variability of Greenland ice losses from satellite gravimetry. *J. Geophys. Res.*, **116**, B07406, 1–11, (doi:10.1029/2010JB007789)

Flechtner (2007) AOD1B Product Description Document (2007). *GR-GFZ-AOD-0001, GeoForschungszentrum, Potsdam, Germany*

Ivins ER, James TS, Wahr J, Schrama EJO, Landerer FW, Simon K (2012) Antarctic Contribution to Sea-level Rise Observed by GRACE with Improved GIA Correction, *J. Geophys. Res.*, In Press, (2012JB009730)

Jacob T, Wahr J, Pfeffer WT and Swenson S (2012) Recent contributions of glaciers and ice caps to sea level rise. *Nature*, **482** (7386) 514–518 (doi:10.1038/nature10847)

King MA, Bingham RJ, Moore P, Whitehouse PL, Bentley MJ, and Milne GA (2012) Lower satellite gravimetry estimates of Antarctic sea–level contribution *Nature*, **49**, 586–589 (doi:10.1038/nature11621).

Klees R, Revtova EA, Gunter BC, Ditmar P, Oudman E, Winsemius HC and Savenije HHG (2008) The design of an optimal filter for monthly GRACE gravity models. *Geophys. J. Int.*, **175**, 417–432.

Larsen CF, Motyka RJ, Freymueller JT, Echelmeyer KA and Ivins ER (2005) Rapid viscoelastic uplift in southeast Alaska caused by post-Little Ice Age glacial retreat. *Earth and Planet. Sc. Lett.*, **237**(3–4), 548–560

Lemoine FG, and many others (1998) The Development of the Joint NASA GSFC and the National Imagery and Mapping Agency (NIMA) Geopotential Model EGM96. **NASA/TP-1998-206861**, NASA Goddard Space Flight Center, Greenbelt, MD 20771.

Luthcke, SB, Zelensky NP, Rowlands DD, Lemoine FG, Williams TA (2003) The 1-Centimeter Orbit: Jason-1 Precision Orbit Determination Using GPS, SLR, DORIS and Altimeter Data. *Marine Geodesy*, **26**, 399-421 (doi:10.1080/01490410390256727).

Luthcke, SB, Zwally HJ, Abdalati W, Rowlands DD, Ray RD, Nerem RS, Lemoine FG, McCarthy JJ and Chinn DS (2006a) Recent Greenland Ice Mass loss by drainage system from Satellite gravity observations. *Science*, **314** (5803), 1286–1289.

Luthcke SB, Rowlands DD, Lemoine FG, Klosko SM, Chinn D and McCarthy JJ (2006b) Monthly spherical harmonic gravity field solutions determined from GRACE inter-satellite range-rate data alone, *Geophys. Res. Lett.*, **33**, L02402 (doi:10.1029/ 2005GL024846).

Luthcke SB, Arendt AA, Rowlands DD, McCarthy JJ and Larsen CF (2008) Recent glacier mass changes in the Gulf of Alaska region from GRACE mascon solutions, *J. Glaciol.*, **54**, 767–777.

Luthcke SB, Sabaka TJ, Loomis BD, Arendt AA, McCarthy JJ, Camp J (2013) Antarctica, Greenland and Gulf of Alaska land ice evolution from an iterated GRACE global mascon solution, *J. Glaciol.*, **In Review**.

Paulson A, Zhong S and Wahr J (2007) Inference of mantle viscosity from GRACE and relative sea level data. *Geophys. J. Int.*, **171**, 497–508.

Rowlands DD, Luthcke SB, Klosko SM, Lemoine FG, Chinn DS, McCarthy JJ, Cox CM and Anderson OB (2005) Resolving mass flux at high spatial and temporal resolution using GRACE intersatellite measurements, *Geophys. Res. Lett.*, **32** (L04310), (doi:10.1029/2004GL021908).

Rowlands DD, Luthcke SB, McCarthy JJ, Klosko SM, Chinn DS, Lemoine FG, Boy J–P and Sabaka T (2010) Global mass flux solutions from GRACE; a comparison of parameter estimation strategies: mass concentrations versus Stokes coefficients, *J. Geophys. Res.*, **115**, B01403, (doi:10.1029/2009JB006546).

Sabaka TJ, Rowlands DD, Luthcke SB and Boy J–P (2010) Improving global mass-flux solutions from GRACE through forward modeling and continuous time-correlation, *J. Geophys. Res.*, **115**, B11403, (doi:10.1029/2010JB007533).

Seber GAF and Wild CJ (1989) Nonlinear regression, 768 p., Wiley and Sons, New York

Schaefer JR, Bull K, Cameron C, Coombs M, Diefenbach A, Lopez T, McNutt S, Neal C, Payne A, Power J, Schneider D, Scott W, Snedigar S, Thompson G, Wallace K, Waythomas C, Webley P and Werner C (2012) The 2009 eruption of Redoubt Volcano, Alaska, *Report of investigations 2011-5*, State of Alaska Department of Natural Resources.

Shepherd A. and many others (2012) A Reconciled Estimate of Ice-Sheet Mass Balance. *Science*, **338** (1183), (DOI: 10.1126/science.1228102).

Schrama EJO and Wouters B (2011) Revisiting Greenland ice sheet mass loss observed by GRACE. *J. Geophys. Res.*, **116**, B02407, (doi:10.1029/2009JB006847)

Swenson S and Wahr J (2002) Methods for inferring regional surface-mass anomalies from Gravity Recovery and Climate Experiment (GRACE) measurements of time-variable gravity. *J. Geophys. Res.*, **107**, B9, 2193, (doi:10.1029/2001JB000576)

Swenson S and Wahr J (2006) Post-processing removal of correlated errors in GRACE data. *Geophys. Res. Lett.*, **33**, L08402, (doi:10.1029/2005GL025285)

Swenson S, Chambers D and Wahr J (2008) Estimating geocenter variations from a combination of GRACE and ocean model output. *J. Geophys. Res.*, **113**, B08410, (doi:10.1029/2007JB005338)

Tapley BD, Bettadpur S, Ries JC, Thompson PF and Watkins MM (2004) GRACE Measurements of Mass Variability in the Earth System. *Science*, **305**, 503–505, (doi: 10.1126/science.1099192)

Truffer M, Harrison WD and March RS (2005) Record negative glacier balances and low velocities during the 2004 heat wave in Alaska: Implications for the interpretation by Zwally and others in Greenland, *J. Glaciol.*, **51**(175), 663.

Velicogna I (2009) Increasing rates of ice mass loss from the Greenland and Antarctic ice sheets revealed from GRACE. *Geophys. Res. Lett.*, **36**, L19503, (doi:10.1029/2009GL040222)

Hoffmann-Wellenhof B and H Moritz (2005) *Physical geodesy*, Vienna, Springer-Verlag.

M. Wolff (1969) Direct Measurements of the Earth's Gravitational Potential Using a Satellite Pair. *J. Geophys. Res*, **74**(22), 5295-5300.